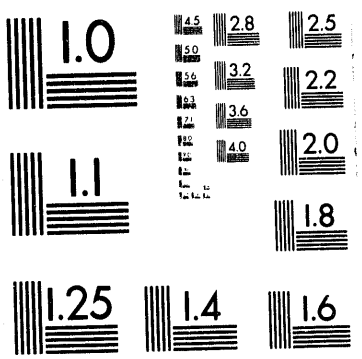
1.0
1.1
1.25
1.4
1.6
1.8
2.0
2.2
2.5
2.8
3.2
3.6
4.0
4.5
5.0
5.6

1 of 1

A SAR image-formation algorithm that compensates for the spatially-variant effects of antenna motion

B. L. Burns and J. T. Cordaro

Sandia National Laboratories
P. O. Box 5800, Albuquerque, NM, 87185-0529

ABSTRACT

A synthetic aperture radar (SAR) obtains azimuth resolution by combining data from a number of points along a specified path. Uncompensated antenna motion that deviates significantly from the desired path produces spatially-variant errors in the output image. The algorithm presented in this paper corrects many of these motion-related errors. In this respect, it is similar to time-domain convolution, but it is more computationally efficient.

The algorithm uses overlapped subapertures in a three-step image-formation process: coarse-resolution azimuth processing, fine-resolution range processing, and fine-resolution azimuth processing. Range migration is corrected after the first stage, based on coarse azimuth position. Prior to the final azimuth-compression step, data coordinates are determined to fine resolution in range and coarse resolution in azimuth. This coordinate information is combined with measured motion data to generate a phase correction that removes spatially-variant errors. The algorithm is well-suited for real-time applications, particularly where large flight-path deviations must be tolerated.

2. INTRODUCTION

SAR image formation can be viewed as the process of compressing a return signal by correlating it with a reference point-target response. In principal, the most general SAR algorithm, time-domain convolution, computes an exact reference function and correlation for every image pixel. Other methods make approximations that trade performance for reduced complexity. These various algorithms differ in how they model the reference function and how they implement the correlation. Much of the difference in reference functions is due to operating conditions (radar frequency, aircraft vs. satellite platforms) and image requirements (size, resolution). Correlator implementation is affected by a number of factors including complexity of the reference function, processing-time requirements, and availability of radar and signal-processing hardware. No single image-formation technique is appropriate for all applications.

The overlapped-subaperture (OSA) algorithm discussed in this paper was designed for real-time, fine-resolution operation in an environment where the radar platform experiences significant off-track motion. Because of the real-time aspect, the algorithm is constructed largely with FFT and vector-multiplication operations. This is important since available DSP chips can compute FFTs quickly and manipulate data as vectors. Some motion-compensation steps are carried out before the return signal is digitized. This motion compensation is implemented by changing the radar frequency, phase, PRF, and A/D sample rate on a pulse-to-pulse basis. The radar computes these parameters as functions of motion data measured by an inertial navigation system. To provide fine resolution in range, the range reference function needs to vary with azimuth position as well as range. The initial stage of OSA processing filters the input data into Doppler-frequency bands corresponding to coarse azimuth position. Filtering at this point increases computational efficiency, because it limits the overall Doppler bandwidth and permits a reduction in the azimuth data rate. Since the radar transmits a linear-FM pulse and de-chirps at the receiver, the range coordinate of a target point is transformed into frequency. In this domain the range correlation consists of a simple frequency shift, carried out by a vector multiplication, followed by an FFT. For the procedure to give acceptable results, the coarse azimuth resolution must satisfy a constraint discussed below.

The azimuth reference function includes terms that depend on range and azimuth pixel coordinates. In addition to the usual along-track motion terms, the reference function contains expressions that account for off-track motion. The navigator system computes geometric parameters that characterize the off-track motion. Since azimuth processing occurs in the time domain, these parameters go directly into the reference function. Correlation with the azimuth reference function occurs at the last processing stage where pixel coordinates are determined to fine resolution in range and coarse resolution in azimuth.

This work was supported by the United States Department of Energy under Contract DE-AC04-94AL85000.

Azimuth correlation consists of a vector multiplication followed by a chirp-z transform (CZT). Use of the CZT here instead of an FFT improves the geometric quality of the image, by keeping the azimuth pixel spacing constant as a function of range.

In what follows, we describe the OSA algorithm and its limitations in more detail. The hardware implementation of the algorithm and quality of the images are interesting topics, but they are not the main subject. This paper emphasizes the aspects of the algorithm that make it tolerant to flight-path deviations. The initial section discusses the parts of motion compensation that are done in real time. The remaining sections deal with the three algorithm stages: coarse-resolution azimuth processing, fine-resolution range processing, and fine-resolution azimuth processing. Figure 1 is a simple block diagram of the OSA method.

Figure 1. Overlapped Subaperture Block Diagram

3. REAL-TIME MOTION COMPENSATION

The amount of digital processing is reduced if the radar performs some motion-compensation operations before digitizing the return signal. This involves changing the frequency and phase of the transmit and receive chirps and varying the sample rate of the A/D, all as functions of antenna motion. A digital waveform synthesizer generates the chirp signals. For the n^{th} pulse, both signals have the form

$$w(t,n)= g(t)\cos(2\pi f_n t + \pi\gamma t^2 + \xi_n), \tag{1}$$

where f_n is the starting frequency, ξ_n is the starting phase, γ is the chirp rate, and g(t) is a gating function.

To see why it is useful to vary f_n and ξ_n, consider the geometry in Figure 2. Let r_s be the range from the radar to some point s in a ground patch, and let r_c be the range to the patch center. Also let ψ be the depression angle between the XY plane and the line joining the radar and patch center. If f_n and ξ_n are constant, the dechirped return signal has Doppler-frequency and range components that are proportional to r_c. These components need to be removed eventually, since the algorithm estimates the range and azimuth coordinates of a point s by operating on the difference

$$r_{sc} = r_s - r_c. \tag{2}$$

A signal processor can accomplish the subtraction in (2) by multiplying the sampled return by appropriate vectors. The disadvantage is that the radar needs to have excess bandwidth to accommodate the variation in r_c. A much better approach is to change the dechirp waveform as a function of r_c. By appropriately incrementing the starting frequency and phase of the receiver chirp, the radar produces the baseband point-target response

$$x_s(t,n) = e^{-\frac{j4\pi r_{sc}}{c}\left[f_{o,n}+\gamma(t-t_o)\right]}, \tag{3}$$

where $f_{o,n}$ is the radar center frequency, and t_o is a constant. For simplicity, we have omitted from (3) the signal amplitude and a phase expression that varies slowly with n.

This first motion-compensation step is adequate for many situations. However, for fine-resolution and/or squint-mode imaging two other steps are helpful to reduce the variation in $x_s(t,n)$ due to r_{sc}. Let $s = (s_a, s_r, s_z)$ denote the azimuth, ground-range, and vertical coordinates of s measured with respect to the patch center. Then the first few terms in an expansion for r_{sc} can be written as

$$r_{sc} \cong s_r \cos\psi - s_z \sin\psi - s_a \alpha \cos\psi \left(1 - \frac{s_r \cos\psi}{r_c}\right) + \ldots . \tag{4}$$

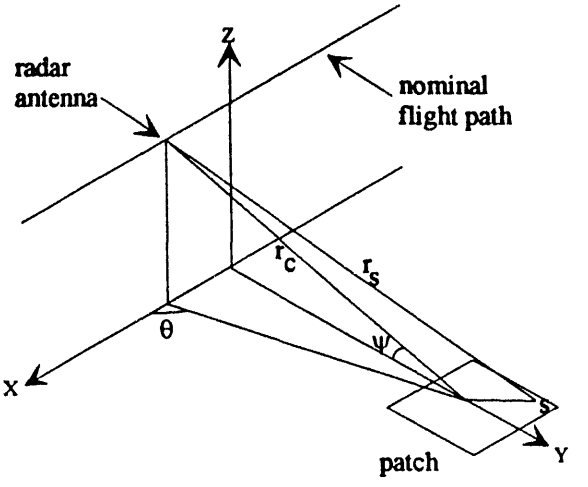

Figure 2. Imaging Geometry

The variable α in (4) is the change in squint angle θ during the aperture. As a second element of motion compensation, the radar adjusts the PRF so that α changes in constant increments as a function of n.

The third element of real-time motion compensation involves the $\cos\psi$ in the equation for r_{sc}. When s_r is large enough, the leading term in (4) can vary by more than a range bin. For broadside imaging, this usually occurs as a consequence of cross-track motion. For squint-mode imaging, $\cos\psi$ has a large linear component even without off-track motion. The range-migration correction described below is a function of s_a but not s_r, so the range correlation implemented by the algorithm cannot deal with significant variations in $s_r\cos\psi$. Azimuth correlation can account for the expression, but the $\cos\psi$ increases Doppler bandwidth, particularly in squint-mode conditions. Both these reasons, suggest dividing r_{sc} by $\cos\psi$[1].

Equation (3) shows that one way to do this scaling in real time is to make the center frequency and either γ or the A/D sample period proportional to $1/\cos\psi$. For hardware reasons, we decided to use the sample period instead of the chirp rate. Since the RF bandwidth requirements increase when the center frequency changes, we have attempted to limit $f_{0,n}$ by setting it to

$$f_{0,n} = f_0 \left(\frac{\cos\psi_0}{\cos\psi}\right), \tag{5}$$

where f_0 is a nominal center frequency, and ψ_0 is the depression angle at the beginning of the aperture. An equation similar to (5) holds for the A/D sample period. The total change in center frequency or sample period increases rapidly for squint angles away from broadside ($\theta = \pm 90°$). This is a disadvantage of real-time scaling. In the case where the radar flies along a line parallel to the x axis, the linear change in the cosine ratio is

$$d\left(\frac{\cos\psi_0}{\cos\psi}\right) \cong \frac{\lambda w_a \cos\psi_0 \tan^2\psi}{2\rho_a \tan\theta}, \tag{6}$$

where λ is the RF wavelength, w_a is the azimuth window bandwidth in bins, and ρ_a is the azimuth resolution. The change in the ratio is larger at fine resolution and low frequency, since the aperture is longer. For squint angles near broadside, the expression in (6) is negligible, and it is necessary to consider a quadratic variation. We will omit the results here.

Let r_{sc}' be the product of r_{sc} and the cosine ratio factor,

$$r_{sc}' \cong s_r \cos\psi_o - s_z \cos\psi_o \tan\psi - s_a \alpha \cos\psi_o \left(1 - \frac{s_r \cos\psi}{r_c}\right) + \ldots . \tag{7}$$

Also let T_F be the nominal A/D sample period, FI a sample index, and F the number of samples per return pulse. Then from (3), the sampled point-target response is

$$x_s(FI, n) = e^{-\frac{j4\pi r_{sc}'}{c}\left[f_o + \gamma T_F\left(FI - \frac{F}{2}\right)\right]}. \tag{8}$$

The processor correlates the return signal with $x_s(FI,n)$. To simplify range correlation, the algorithm compensates for the range migration due to the third term in (7), and neglects higher-order terms. This is an approximation that is appropriate in many situations. For azimuth correlation, the algorithm includes higher-order terms that are functions of α, as well as ψ and r_c. The last two are important when the radar experiences off-track acceleration.

Real-time motion-compensation based on r_c and ψ is best for the OSA algorithm when operating conditions call for spotlight or squint modes. This approach to motion compensation has been assumed in the discussion which follows; however, the algorithm described can be modified if the motion compensation described above is not available. One example is a broadside geometry where motion compensation is based on the range and depression angle to a line through the patch center rather than to a point at the patch center. The benefit of the algorithm is maintained in this situation.

4. COARSE-RESOLUTION PROCESSING

Each dechirped return pulse is sampled F times, digitized, and read into the first corner-turning memory CTM0 as an Fx1 complex vector. The first processing stage filters the sampled data into Doppler frequency bands that correspond to coarse azimuth position. Overlapped FFTs realize the filtering. Figure 3 is a block diagram of coarse-resolution processing showing the memory CTM0, along with vector multiplies and an FFT. The signal generator is a chirp synthesizer used in the case where r_c is not subtracted out of the signal phase at an earlier stage.

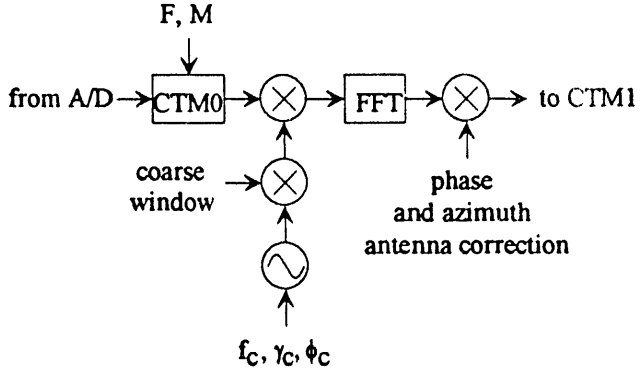

Figure 3. Coarse-Resolution Processing

Data in the corner-turning memory are arranged into FxM matrices, called subapertures. Azimuth samples in the subapertures are overlapped as indicated in Figure 4. The total number of return pulses N_a and the number of subapertures S are related by

$$N_a = (S - 1)\Delta + M, \tag{9}$$

where Δ is the number of azimuth samples between subapertures.

Coarse-resolution processing operates on 1xM row vectors from a subaperture. Each row vector is shifted in frequency, windowed, and Fourier transformed. By transforming sequences of overlapped 1xM vectors, the first processing stage implements a bank of bandpass filters, followed by a decimation in time. The decimation factor is Δ, since as indicated by (9), $S \cong N_a/\Delta$. Efficiency considerations suggest making Δ as large as possible. However, the bandpass decimator introduces aliased azimuth sidelobes into the Doppler spectrum that are spaced $1/\Delta$ apart in normalized frequency, so Δ is limited by a function of the bandwidth of the window function. For a -50 dB Taylor window and peak aliased azimuth sidelobe energy of -40 dB, an upper limit on Δ is

$$\Delta \leq \frac{M}{2.58}. \tag{10}$$

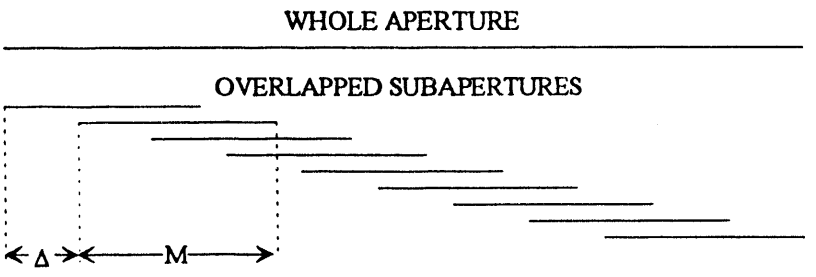

Figure 4. Overlapped Subapertures

The choice of M has a significant effect on the total number of operations required to form an image. Let δ_{ca} be the azimuth resolution corresponding to the bandwidth of a Doppler bin. M and δ_{ca} are inversely proportional. The minimum value of δ_{ca} is limited by a range-walk constraint. At the coarse-resolution stage, range-walk due to the third expression in (7) has not been compensated. Points at the azimuth edge of a ground patch will move in range during a coarse-resolution interval, and M needs to be small enough that the motion is less than one range cell. This results in a lower bound on δ_{ca}. Let P_a be the azimuth size of a patch. Then to limit the range walk to one range cell, δ_{ca} should satisfy

$$\delta_{ca} \geq \frac{\lambda P_a}{4\rho_r}, \tag{11}$$

where ρ_r is the range resolution[1].

After the FFT, the data are corrected for the azimuth antenna pattern. If the output images are for a SAR interferometry application, a correction for the phase introduced by the FFT is applied here also. Since the azimuth sample rate is chosen to oversample the Doppler spectrum, the outputs of some filters correspond to points outside the ground patch of interest. Only A < M coarse-resolution bins need to be saved, where A is proportional to the azimuth patch size. A is typically less than one-half M, so memory size is reduced at an early stage. If the effect of $\cos\psi$ on the Doppler bandwidth had not been removed, A would need to be larger; however the algorithm still functions correctly. The memory reduction is significant for squint-mode imaging with large range swath.

Following the antenna-pattern correction the 1xA row vectors are read into the second corner-turning memory, CTM1. These rows form an FxA matrix in CTM1. The input data for coarse-resolution processing can be thought of as an FxN_a complex matrix. The output is a sequence of S matrices each of dimension FxA. We will not show it here, but N_a is on the order of S·A. So this first processing stage divides the input data into coarse azimuth bins with only a slight increase in the total amount of data.

5. RANGE PROCESSING

For range processing, Fx1 column vectors are read from CTM1. Each subaperture has a total of A such vectors. The correlation that is carried out at this stage consists of vector multiplications and FFTs, as indicated in Figure 5. There are two basic parts. First, each column is multiplied by a different range-walk correction vector. This compensates the linear range variation over an aperture as a function of coarse azimuth position. Since the radar transmits a linear-FM waveform

and dechirps the return pulse, range appears in these column vectors as frequency. So a range translation corresponds to a simple frequency shift. The second part of the correlation is just an FFT.

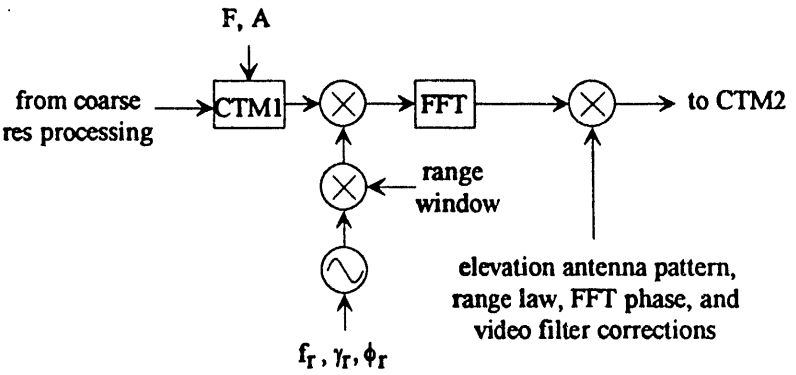

Figure 5. Range Processing

The range-walk correction involves an approximation. As shown by (7), the amount of range walk is a function of the azimuth coordinate s_a. Suppose we divide the azimuth width of the patch into intervals of width δs_a and use the azimuth coordinate at the center of each interval to construct a correction vector. Data from points at the center of an interval will be compensated correctly while that from the edges will have some residual range walk. The impulse response function is widened by about 4% when the residual error is one range resolution cell. To hold the maximum error at one cell or less, δs_a is constrained by the inequality

$$\delta s_a \le \frac{4\rho_a\rho_r}{\lambda w_a}. \tag{12}$$

A small range dependence is ignored in (12).

The size of δs_a relative to the width of a coarse bin affects how the correction vector is applied. If $\delta_{ca} \le \max(\delta s_a)$, then one correction vector per bin is sufficient. This is the simplest case. On the other hand, if $\delta_{ca} > \max(\delta s_a)$, then each Fx1 input column must be multiplied by more than one correction vector, and the resulting vectors saved for the remaining processing steps. This case is less desirable because the amount of processing is greater. For example, if it is determined that two corrections need to be applied to each input vector, the FxA input array expands to Fx(2A). Since the minimum value of δ_{ca} is limited by (12), some combination of radar parameters make the multiple-correction situation necessary. However, to simplify our discussion, we will deal with the single-correction case.

For each Fx1 input vector, the correction function is a constant-frequency complex exponential, which is generated easily by the digital synthesizer shown in Figure 5. If r_c has not been subtracted from the return-signal phase in real time, it can be included in the frequency shift. After multiplication by the correction and window functions, the resulting vector is Fourier transformed. At this point range is determined to fine resolution. The output is corrected for the roll-off in elevation antenna pattern, range path loss, video filter response, and FFT phase components. Only R range bins are saved where R is less than or equal to the number of samples in the FFT output. This allows an adjustment in range pixel spacing, since the return pulse may be oversampled. The output from range processing is a sequence of Rx1 column vectors that are loaded into a third corner-turning memory, CTM2. The range index is RI in figures which follow.

The flow of data from the processor input to the output image is illustrated in Figure 6. Notice that the coarse-azimuth and fine-range stages operate on subapertures. With real-time pipelined processing, subapertures flow through these two stages into CTM2 as the aperture is flown. Each RxA matrix in CTM2 is a complex image having coarse resolution in azimuth and fine resolution in range as shown in Figure 7. There are S of these images during the synthetic aperture. One of the most significant benefits of OSA processing is that unique fine-resolution focus vectors are computed for each cell in Figure 6 during the fine-resolution correlation operation. This focusing operation corrects for range and azimuth dependent effects of non-ideal motion.

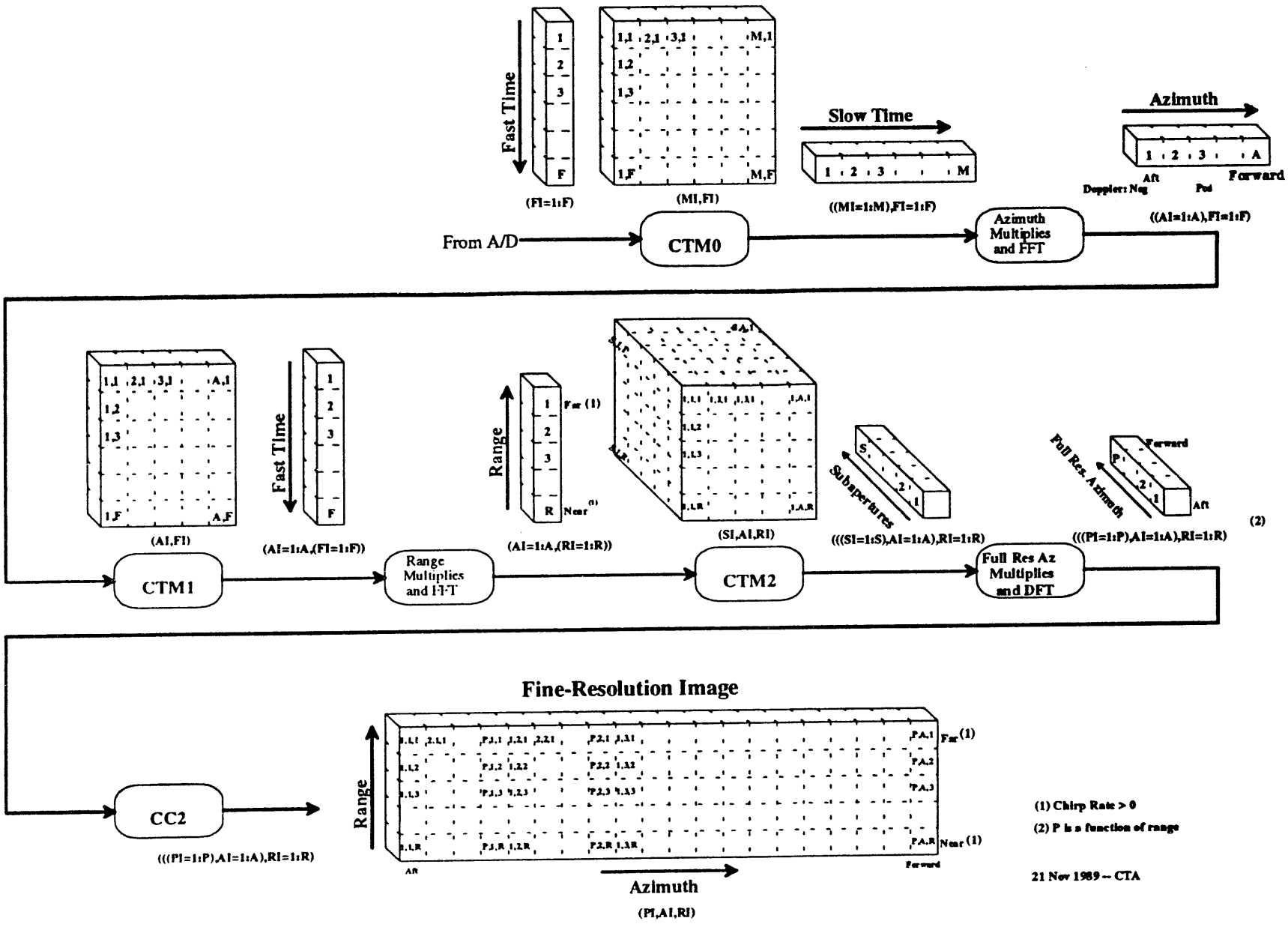

Figure 6. Data Flow

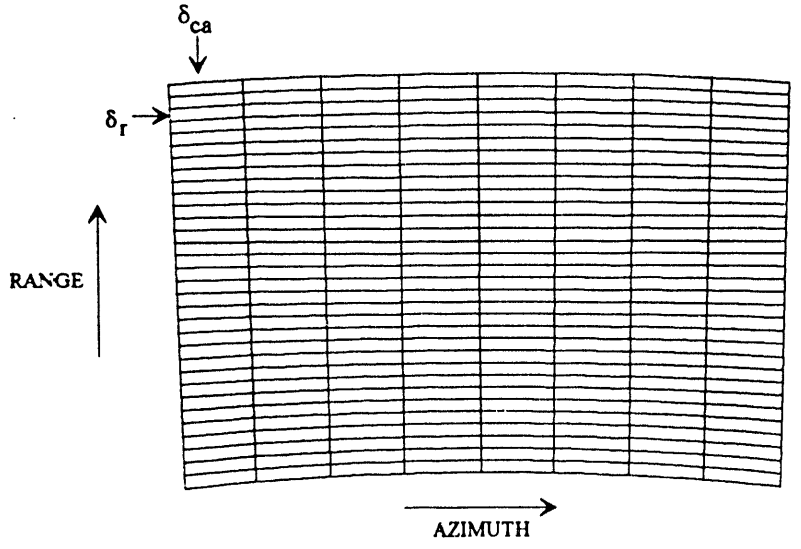

Figure 7. Range and azimuth representation of coarse-resolution image.

6. FINE-RESOLUTION AZIMUTH PROCESSING

The azimuth correlation implemented at the last processing stage consists of vector multiplications and FFTs. However, for at least three reasons, the situation is more complicated than for range correlation. First, the correction function applied to the input vector depends on measured antenna position in addition to range and coarse-azimuth coordinates. Second, navigator-system errors produce an azimuth phase error that must be estimated by an autofocus technique and included in the correction function. Finally, the processor needs to adjust the frequency band and sample spacing in the azimuth correlation as functions of range.

Up to this point, the algorithm has dealt with each subaperture separately. Now processing extends across subapertures. All the return pulses must be processed by the first two stages before this last stage can begin. The input to fine-resolution azimuth processing is a length-S vector read from CTM2 for fixed range and azimuth bins. Figure 6 shows CTM2 as a three-dimensional array, indexed by coarse-azimuth, range, and subaperture. Figure 8 is a diagram of fine-resolution azimuth processing. Since the chirp-z transform (CZT) is computed with three FFTs, the basic elements in the diagram are again complex multiplies and FFTs. The correction function before the CZT is divided into three parts: quadratic focus, higher-order focus and autofocus. This particular division is based on how the processor generates each part.

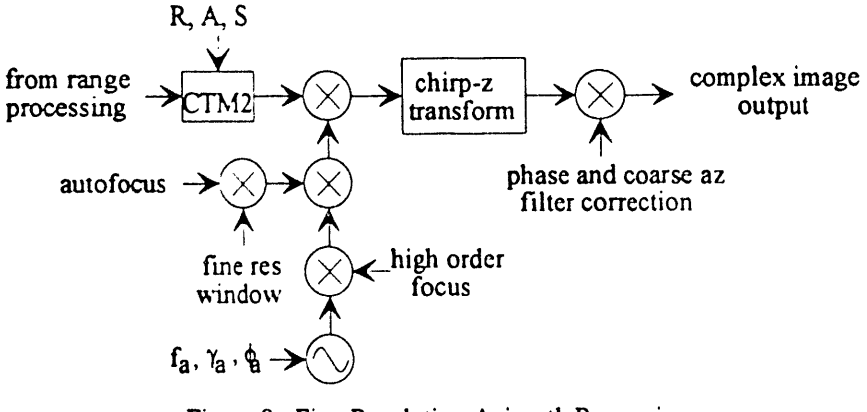

Figure 8. Fine-Resolution Azimuth Processing

6.1. Focus Vectors

The azimuth correlation function includes terms in r_{sc}' that are not shown in (7). Some of these consist of expressions that are quadratic or cubic in α. For convenience, we have grouped the quadratic components with another function needed for the CZT and generated the resulting chirp waveform with the synthesizer in Figure 8. For this, the control program computes a starting frequency f_a, chirp rate γ_a, and starting phase ϕ_a repeatedly as functions of range and coarse azimuth position. An expression that is cubic in α is placed in the high-order focus vector.

For squint mode and/or situations with off-track motion, the azimuth correlator needs to account for variations in r_c and ψ that occur during an aperture. One expression in r_{sc}' that does this is

$$h(SI) = \cos\psi_0 \frac{s_r^2 \sin^2\psi + s_a^2}{2 r_c \cos\psi}\left(1 - \frac{s_r \cos\psi}{r_c}\right), \tag{13}$$

where SI is the subaperture index. Both r_c and ψ are estimated by the navigator system as functions of SI. Since the correlator operates in the time domain, it uses r_c and ψ directly. Whether or not more terms are needed to describe the phase of the point-target return depends on several factors including the patch size, range, wavelength, and resolution. We will limit the discussion to h(SI).

The function h(SI) contributes a phase of $4\pi h(SI)/\lambda$ to the exponent of the point-target response. Linear components in this phase expression shift the impulse-response function in azimuth position. Since the amount of shift depends on the target coordinates s_r and s_a, these linear components distort the image instead of simply translating it. The effect is most noticeable for squint mode, but even for $\theta = 90°$, off-track motion can produce a skewing in the image. The algorithm correlates the return signal with the linear components by adjusting the frequency band over which it computes the CZT.

Higher-order components in h(SI) are not separated into powers of SI. The algorithm simply computes a complex exponential with the appropriate phase and makes it part of the higher-order focus vector shown in Figure 8. This is the advantage of having fine range and coarse azimuth coordinates available before azimuth correlation.

To judge whether or not h(SI) matters in a particular application we need to look at its behavior in more detail. If radar motion is only in the along-track direction, h(SI) has a quadratic component that can be significant. For example, the peak quadratic phase due to the s_a-dependent part of (13) is

$$Q_{xa} = \frac{s_a^2 \pi \lambda w_a^2 \cos\psi_0 \left(3\cos^2\theta - 1\right)}{16 r_c \rho_a^2 \sin^2\theta \cos^3\psi}. \tag{14}$$

Usually, the peak quadratic error allowed is in the range of 60° to 90° based on image quality constraints. If Q_{xa} is small enough for some set of parameters, it can be neglected.

Off-track motion increases the phase variation. Suppose the aircraft acceleration is constant during an aperture and equal to a_y and a_z along the Y and Z axes. Also, let v_x be the along-track velocity. Then, neglecting the last expression in parentheses in (13), the peak quadratic phase due to the range-dependent part of h(SI) is

$$Q_r = s_r^2 \pi \lambda \cos\psi_0 \left[\frac{w_a}{4\rho_a v_x \sin\theta}\right]^2 \left[a_y \tan^2\psi \sin\theta\left(1 + 2\cos^2\psi\right) + 2a_z \cos\psi \sin\psi\right]. \tag{15}$$

Since (15) is not a function of r_c, increasing the operating range does not reduce Q_r. The dependence on a_z is probably not important because we attempt to fly at a constant altitude during a synthetic aperture. In this case, vertical motion is largely due to turbulence, and the average a_z is nearly zero. However, the part of (15) that is a function of a_y models the realistic situation where the aircraft turns during an aperture.

The peak quadratic phase due to the s_a-dependent part of off-track acceleration is

$$Q_a = \frac{s_a^2 \pi \lambda w_a^2 a_y \cos\psi_o}{\sin\theta (4\rho_a v_x \cos\psi)^2}. \tag{16}$$

Since OSA processing determines s_a to coarse resolution, the error in s_a^2 is approximately $s_a \delta s_a$. After multiplication by the fine-resolution focus vector, points at the edge of a coarse bin have residual errors of $(\delta s_a/s_a)Q_{xa}$ and $(\delta s_a/s_a)Q_a$.

Another SAR algorithm would need some amount of range and azimuth resolution before the final azimuth compression stage to compensate the changes in h(SI). An algorithm that does range compression before azimuth compression should be able to compensate for Q_r. Algorithms that cannot compensate for Q_{xa} and Q_a need to restrict some of the parameters in (14) and (16) to keep the errors at a tolerable level.

For a strip-map application, processing efficiency is enhanced if the azimuth patch size is at least equal to the synthetic aperture length. This requires that the maximum s_a increase linearly with wavelength. In this case, since Q_{xa} and Q_a are functions of the product $s_a^2\lambda$, the wavelength dependence of the maximum of either error is proportional to λ^3.

6.2 Autofocus

The variables estimated by the navigator system contain errors that affect image quality. The dominant error comes from the motion-compensation step that subtracts r_c from the return signal phase. Since this operation applies equally to all target points, the resulting error is a function of SI but not of s_r or s_a. The processor incorporates the Phase Gradient Autofocus[2] (PGA) algorithm to estimate and remove this phase error. Figure 8 omits the PGA structure and shows the output from autofocus as a single component of the focus vector.

Implementation of an autofocus algorithm within OSA processing has some advantages. Potential autofocus inputs include all the length-S vectors in CTM2. Because of the coarse-resolution stage, it is usually possible to limit the number of input vectors to a few having sufficiently high signal-to-noise ratio. The signal-to-noise ratio estimate is computed from data flowing out of the range processing of Figure 5. The processor multiplies these selected inputs by the quadratic and high-order focus vectors, so spatially-variant errors are compensated prior to autofocus processing. This is an important aspect, since PGA assumes the phase error in each input is the same. Finally, the fact that the input vectors have length S instead of N_a reduces the autofocus computation requirement substantially.

6.3 Height of focus

After multiplication by the azimuth correction function, the dominant phase variation in the point-target response is due to the second and third terms in r_{sc}'. The first of these, $s_z\cos\psi_0\tan\psi$, is a function of s_z. Since s_z is not resolved by 2-D SAR, the azimuth correlation simply ignores it. To describe the effect of this term on the image, we need to define the slant plane. This is the plane containing the patch center and a nominal flight path parallel to the x axis. Briefly, if the aircraft remains in the slant plane during an aperture, the term does not widen the azimuth response. Motion out of the slant plane can defocus the image. For example, assume the off-track velocity components are small compared with V_x, and the acceleration normal to the slant plane is a constant a_n. Then the expression produces a quadratic phase with peak value

$$Q_z = s_z \frac{\pi \lambda r_c a_n \cos\psi}{8\cos\psi_o \cos\phi}\left(\frac{w_a}{\rho_a v_x \sin\theta}\right)^2, \tag{17}$$

where ϕ is the angle between the slant and XY planes. In general, the height-of-focus is the range of s_z values for which Q_z is less than some acceptable value.

6.4 Azimuth correlation DFT

Neglecting the phase errors mentioned above, the last remaining phase variation in the point target response comes from the third expression in (7). Since it is linear in α, the final step in azimuth correlation can be computed as a discrete Fourier transform (DFT). In computing this transform, it is necessary to account for the range dependence indicated in (7). This is done simply with the CZT. If the range dependence ignored, the correlation will be with Doppler frequency instead of azimuth position, and the resulting image will need to be resampled from a Doppler-frequency grid to an azimuth-position grid.

For each range bin and a sequence of adjacent coarse bins, the processor reads an S-vector from CTM2, multiplies it by the correction vector, and computes its DFT over a specific frequency band. The exact frequency band is a function of range and coarse-azimuth bin numbers. Use of the CZT instead of an FFT makes this calculation straightforward, since precise frequency limits can be specified[3]. However, other DFT implementations such as mixed-radix FFTs may be used with appropriate modifications to the synthesizer frequency, f_a, in Figure 8. A CZT requires multiplications by chirp waveforms and calculation of three FFTs. These operations are readily implemented in typical processor hardware. Since the CZT output sample spacing is only a function of range and not azimuth location, one of the FFTs in the CZT does not need to be recomputed for each coarse-resolution azimuth bin of the processing. This reduces the overhead of using the CZT to perform the final processing step by approximately one-third.

At the very last step, the algorithm corrects the output from each DFT for the amplitude response of the coarse-resolution filters, and for a phase function introduced by the transform. The sequence of outputs from each coarse-resolution bin for a fixed range bin is one line of a complex image as illustrated in Figure 6. Figure 6 illustrates the output from a single coarse-resolution bin as have P samples. The processing is repeated for all ranges to form the complete image.

7. CONCLUSIONS

The OSA algorithm was designed for a real-time, fine-resolution SAR operating in an environment where off-track motion is significant. This paper emphasizes aspects of the algorithm that provide tolerance to flight-path deviations. The first of these is real-time motion compensation. By changing the starting frequency and phase of the waveform synthesizer, the A/D sample period, and the PRF as functions of antenna motion, the radar removes many undesired components from the return signal in real time. This simplifies the correlations carried out by the signal processor. The first element of the algorithm is a bandpass filter and decimator that provides coarse azimuth resolution and a data rate reduction. Range correlation at the next stage consists of a frequency shift, realized as a vector multiplication, followed by an FFT. Azimuth correlation involves a phase correction and DFT. Since the phase correction is a function of range and coarse-azimuth position, the correlation includes motion effects that other algorithms neglect.

8. ACKNOWLEDGMENTS

The authors thank Christopher T. Allen for creating Figure 6 which illustrates the flow of data through the processor.

9. REFERENCES

1. J. L. Walker, "Range-Doppler Imaging of Rotating Objects," *IEEE Trans. Aerosp. Electron. Syst.*, vol. AES-16, p. 23, January 1980.

2. P. H. Eichel, D. C. Ghiglia, and C. V. Jakowatz, Jr., " A Speckle Processing Method for Synthetic Aperture Radar Phase Correction," *Optics Letters*, 14, January 1989.

3. L. R. Rabiner and B. Gold, *Theory and Application of Digital Signal Processing*, Prentice Hall 1975, pp393-399.

DISCLAIMER

DATE
FILMED
5/5/94
END